Journal of Power Sources 122 (2003) 37–46

www.elsevier.com/locate/jpowsour

The influence of operating temperature on the efficiency of a combined heat and power fuel cell plant

S.F. Au [a,b,*], S.J. McPhail [b], N. Woudstra [b], K. Hemmes [c]

[a] *Laboratory of Material Science, Delft University of Technology, Rotterdamseweg 137, 2628 AL Delft, The Netherlands*
[b] *Laboratory for Thermal Power Engineering, Delft University of Technology, Mekelweg 2, 2628 CD Delft, The Netherlands*
[c] *Faculty of Technology, Policy and Management, Delft University of Technology, P.O. Box 5015, 2600 GA Delft, The Netherlands*

Received 22 August 2002; received in revised form 3 February 2003; accepted 10 February 2003

Abstract

It is generally accepted that the ideal operating temperature of a molten carbonate fuel cell (MCFC) is 650 °C. Nevertheless, when waste heat utilization in the form of an expander and steam production cycle is introduced in the system, another temperature level might prove more productive. This article is a first attempt to the optimization of MCFC operating temperatures of a MCFC system by presenting a case study in which the efficiency of a combined heat and power (CHP) plant is analyzed. The fuel cell plant under investigation is designed around a 250 kW-class MCFC fuelled by natural gas, which is externally reformed by a heat exchange reformer (HER). The operating temperature of the MCFC is varied over a temperature range between 600 and 700 °C while keeping the rest of the system the same as far as possible. Changes in energetic efficiency are given and the causes of these changes are further analyzed. Furthermore, the exergetic efficiencies of the system and the distribution of exergy losses in the system are given. Flowsheet calculations show that there is little dependency on the temperature in the first order. Both the net electrical performance and the overall exergetic performance show a maximum at approximately 675 °C, with an electrical efficiency of 51.9% (LHV), and an exergy efficiency of 58.7%. The overall thermal efficiency of this CHP plant increases from 87.1% at 600 °C to 88.9% at 700 °C. Overall, the change in performance is small in this typical range of MCFC operating temperature.

Keywords: Fuel cell; MCFC; Modeling; Flowsheet; Design

1. Introduction

Fuel cells play an important role in the continuing effort to increase the efficiency of electricity production and to reduce atmospheric pollution. High net power efficiency can be achieved thanks to the principle of direct conversion of chemical energy to electrical energy, and thereby avoiding the extra steps of combustion, heat transfer, expansion and generation as in a conventional plant. Furthermore, when high-temperature cells like the molten carbonate fuel cell (MCFC) are used, additional increase in the overall efficiency can be obtained by proficient residual heat utilization. Then, in order for the total efficiency to be as high as possible, it is possible that ideal fuel cell operating conditions will not coincide with the optimal total system performance.

It is generally accepted that the ideal operating temperature of an MCFC is 650 °C. For current state of the art fuel cell, this temperature is the best compromise between performance and endurance [1–3]. Optimization studies of MCFC system efficiencies are therefore done in the fields of cell and stack configuration [4–6] and system configurations [7,8]. However, when waste heat utilization in the form of an expander and steam generation is introduced in the system, another temperature level might prove to be more productive. Previously, we performed a theoretical study to the efficiencies of fuel cell systems using simple assumptions for the irreversible losses [9,10]. The results were obtained by assuming temperature independent losses for the recovery of the exergy of the residual heat. In practice, the efficiency of waste heat recovery depends on the temperature of the system. Furthermore, the interactions between the fuel cell stack, auxiliary equipment and waste heat recovery system were previously neglected. Here, we present more detailed flowsheet calculations of a typical external reformed MCFC combined heat and power (CHP) plant with which we investigate the influence of the fuel

* Corresponding author. Present address: Institute for Materials and Process in Energy Systems, IWV3 Energy Process Engineering, Forschungszentrum Jülich, Jülich D-52425, Germany.
Tel.: +49-2461-615291; fax: +49-2461-616695.
E-mail address: s.f.au@fz-juelich.de (S.F. Au).

0378-7753/03/$ – see front matter © 2003 Elsevier Science B.V. All rights reserved.
doi:10.1016/S0378-7753(03)00345-8

Nomenclature

A_{cell}	active cell area (m^2)
C_i	fitting constant for quasi-ohmic resistance ($\Omega\,m^2$)
d	electrolyte thickness (mm)
d_b	normalization constant for the electrolyte thickness (mm)
Ex	exergy (kW)
Δh_i	activation enthalpy (J/mol)
i_{cell}	current load density of the unit cell (A/m^2)
m	molar fraction (–)
P	power delivered (kW)
p	pressure (bar)
p_i	partial pressure of gas of species i (bar)
Δp	pressure loss (bar)
r	quasi-ohmic resistance ($\Omega\,m^2$)
R	universal gas constant (J/mol K)
T	temperature (°C)
T_0	standard ambient temperature (°C)
ΔT_{high}	high end temperature difference (K)
ΔT_{low}	low end temperature difference (K)
u	local cumulative fuel utilization (–)
u_f	total fuel utilization (–)
V_{cell}	cell voltage (V)
V_{eq}	Nernst voltage (V)

Greek symbols

Φ	mass flow (kg/s)
η	efficiency (–)
λ	air to fuel ratio (kg/kg)

cell operating temperature on the system performance. This system has been modeled and implemented in the program Cycle-Tempo [11], which is a program that Delft University has developed for flowsheet calculations. The effects of varying the cell temperature upon the fuel cell (both reversible and kinetical) and various system aspects have been investigated, and based on these results, the optimal operating temperature for maximum efficiency will be presented.

2. System configuration

The system selected for this study is similar to a system-design considered for a 250 kW natural gas MCFC system as jointly defined in the past by the Delft University of Technology and ECN (Netherlands Energy Research Foundation) [12]. It has the following main features:

- 250 kW-class CHP system;
- natural gas as primary fuel;
- fuel gas is externally reformed;
- pressurized system operating at 4 bar.

The initially proposed system has an intricate connection between the anode cycle and the cathode cycle (via the preheating stages and mixing). This connection is removed here mainly as regards to stability, constructive simplicity and controllability. Separating the two flows should bring about a better system. Fig. 1 shows the flowsheet of the modified system that is taken directly[1] from the flowsheeting program. The system layout shows that apart from the fuel cell we can distinguish five subsystems. Next, the fuel cell and the subsystems will be introduced by explaining their functions. Furthermore, the input data used for the different components will be presented. These inputs consist of input data that characterize state of the art equipments.

2.1. Fuel cell

A unique feature of the fuel cell model in the flowsheeting program is its capability of calculating design and off design or part load performances, next to the energy and mass transfer calculations. The cell performance is calculated by numerically solving an integral expression for cell voltage V_{cell} as function of the operating parameters fuel utilization u_f and current density i_{cell}

$$V_{cell} = \frac{1}{u_f}\int_0^{u_f} V_{eq}(u)\,du - \frac{r}{i_{cell}}\int_0^1 i^2(x)\,dx \quad (1)$$

where V_{eq} is the Nernst voltage expressed as function of the cumulative local fuel utilization u, $i(x)$ the local current density and r the quasi-ohmic resistance that accounts for all irreversible losses. Therefore, the first integral represents the reversible cell voltage as function gas composition, operating temperature and pressure and total fuel utilization u_f. The second integral represents the irreversible losses due to ohmic losses and electrochemical kinetics as function of mean current density i_{cell}. This is done by assuming a local ohmic relation for the electrode kinetics (see [13]). A detailed description of the complete fuel cell model is given in [14] together with a verification of model by comparing the calculated results with the experimental results obtained from a 110 cm^2 benchmarking class MCFC single cell. Using the measured macroscopic cell resistance[2] as the quasi-ohmic resistance, this verification showed an average relative discrepancy of 0.5% over a wide range of operating condition, and a maximum discrepancy of 3% at full load. Hence, it is shown the fuel cell model is correct and its accuracy sufficient to be used for flowsheeting purposes. This fuel cell model enables us to use the relations for the

[1] Components that are needed solely for starting values of mathematical iterations are removed here.

[2] A small difference in value exists between the quasi-ohmic resistance and the macroscopic cell resistance. The difference is described in detail in [13]. Using the fitted quasi-ohmic resistance, the discrepancy between the calculated and measured cell voltage can be improved to 1.7% at full load (see [14]). The elaborate fitting procedure for the quasi-ohmic resistance is here omitted.

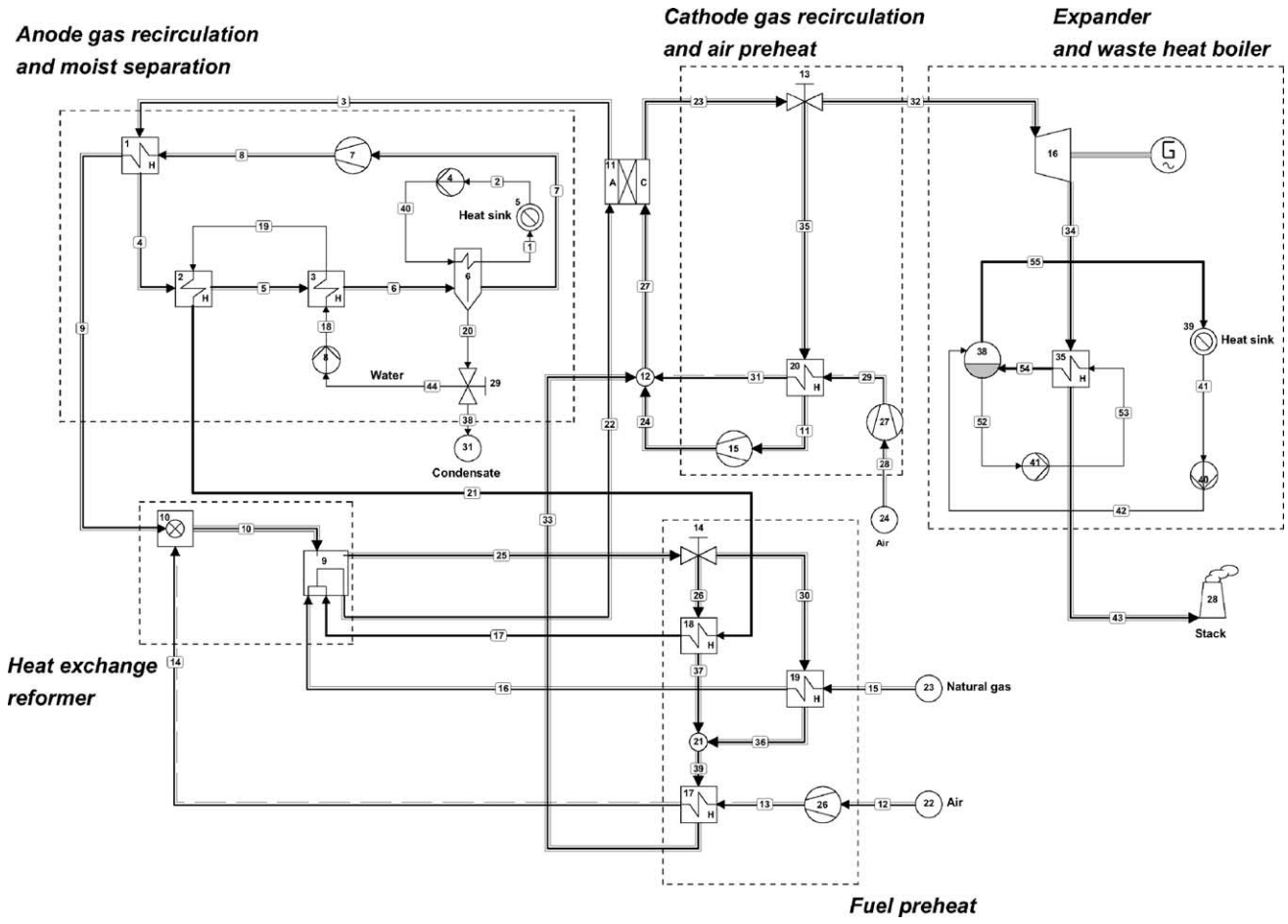

Fig. 1. Flowsheet of the 250 kW-class MCFC CHP plant.

temperature dependency of the macroscopic cell resistance measured by CRIEPI[3] [6,15]. They obtained the following empiric relations for the cell resistances r, which can be distinguished in an anode contribution r_a, an electrolyte resistance r_{ir} and a cathode contribution r_c:

$$r = r_a + r_{ir} + r_c \tag{2}$$

with:

$$r_a = C_a T \exp\left(\frac{\Delta h_a}{RT}\right) \frac{1}{\sqrt{p_{a,H_2}}}, \quad r_{ir} = \frac{d}{d_b} C_{ir} \exp\left(\frac{\Delta h_{ir}}{RT}\right),$$

$$r_c = C_{c1} \exp\left(\frac{\Delta h_{c1}}{RT}\right) \frac{T\sqrt{p_{CO_2}}}{p_{c,O_2}^{0.75}} + \frac{C_{c2} \exp(\Delta h_{c2}/RT) T}{m_{c,CO_2} + C_{c3} \exp(\Delta h_{c3}/RT) m_{c,H_2O}} \tag{3}$$

The symbols C_i, Δh_i and d_b are respectively fitting parameters, activation enthalpy and normalization parameter for the electrolyte matrix thickness with the thickness $d =$ 0.916 mm. The fitting parameters and activation enthalpy are obtained by fitting these empirical relations to experimental measurements performed at a temperature range between 600 and 700 °C, and at a pressure range between 1 and 5 bar. The resulting values are given in Table 1.

The empirical relations are used to calculate the cell resistance as function of cell temperature, pressure and average

Table 1
Values for the fitting parameters for the cell resistance taken from [6,14]

Parameter	Value
C_a	$9.50 \times 10^{-7}\ \Omega\,cm^2$
C_{c1}	$6.91 \times 10^{-15}\ \Omega\,cm^2$
C_{c2}	$3.75 \times 10^{-9}\ \Omega\,cm^2$
C_{c3}	$1.07 \times 10^{-6}\ \Omega\,cm^2$
C_{ir}	$9.48 \times 10^{-3}\ \Omega\,cm^2$
Δh_a	27.9 kJ/mol
Δh_{c1}	179.2 kJ/mol
Δh_{c2}	67.2 kJ/mol
Δh_{c3}	95.2 kJ/mol
Δh_{ir}	23.8 kJ/mol
d_b	0.916 mm

[3] Central Research Institute of Electric Power Industry, Japan.

Table 2
Input parameters of the system

Fuel cell	
A_{cell}	250 m^2
i_{cell}	1500 A/m^2
u_f	70%
η_{dc-ac}	96%
p	4 bar
Δp_{anode}	0.05 bar
$\Delta p_{cathode}$	0.1 bar
$T_{out} - T_{in}$	100 °C
Anode gas recirculation and moisture separation	
T_{out} anode recirculation gas	460 °C
$T_{hot\ water}$	80 °C
$T_{utilization}$	20 °C
ΔT_{low} evaporator	20 °C
Δp heat exchangers	0.05–0.10 bar
Δp moist separator	Primary side 0.15 bar; secondary side 0.1 bar
η_i for pump	0.70
η_i for blower	0.72
Heat exchange reformer and fuel preheat	
λ (air factor) combustor	1.1
Steam to fuel ratio reformer	2.59
T_{react} reformer	800 °C
p_{react} reformer	4 bar
Δp reformer	Primary side 0.5 bar; secondary side 0.25 bar
T_{out} reformer	According to cell inlet temperature
Δp heat exchangers	0.05 bar for both primary and secondary sides
T_{feed} reformer	480 °C
T_{air} combustor	440 °C
η_i compressor	0.72
Cathode gas recirculation	
Δp heat exchanger	0.05 bar for both primary and secondary sides
η_i compressor	0.72
Expander and waste heat boiler	
ΔT_{low} evaporator	20 °C
Δp heat exchanger	Primary side 0.1 bar; secondary side 0.01 bar
Δp utilization	0.2 bar
η_i expander	0.75
η generator	0.9
η_i pumps	0.75

gas composition (by means of average partial pressures p_i and mol fractions m_i). The cell resistance r determines the irreversible losses and therefore the performance of the cell. Changes in reversible heat production and Nernst loss due to temperature and gas compositions changes are accounted by the first integral in Eq. (1) by means of changes in the local Nernst voltages [13]. Note that the symbols p and T in Eq. (3) are used for respectively partial pressure (bar) and absolute temperature (K).

In this study, both the cell area A_{cell} and the current density i_{cell} are kept constant and they are given in Table 2. The power that is delivered by the fuel cell is therefore a function of cell resistance, fuel utilization and gas inlet compositions.[4] Losses due to the dc to ac conversion are introduced by the inverter efficiency η_{dc-ac}. Fuel utilization is fixed at 70%, which is 5% lower than described in [12]. The reason for the low fuel utilization lays solely on the separation of anode and cathode cycles. Due to this separation, extra enthalpy is required in order to heat up the fuel and to provide enough heat for the heat exchange reformer (HER) without subtracting this from the cathode cycle. By reducing the fuel utilization, the fuel input has increased and more heat is available from the anode off gas. Friction losses are introduced by imposing pressure drops of 0.05 and 0.1 bar for the anode and cathode respectively. Co-flow configuration is assumed and the temperature difference between the inlets and the outlets of both the anode and cathode are set at 100 K.

The system is implemented in such a way that the fuel cell is the dominant apparatus and that both fuel and air consumptions are mainly[5] determined by it. Fuel consumption is determined by i_{cell}, A_{cell} and u_f. The cathode mass flow, and the related air consumption, is determined by the heat that must be discharged from the fuel cell.

2.2. Anode gas recirculation and moisture separation

Fuel that is not converted by the fuel cell is combusted in the reformer (HER). However, the anode off gas contains large amount of moisture that will adversely influence the performance of the HER. The anode off gas is therefore cooled in several stages to separate most of the moisture. The transferred heat is used for heating up and evaporating water that is needed for the reforming reaction. Heat released in the moisture separator is utilized by external consumers (e.g. a district heating system) represented here by a heat sink. The moisture separator produces hot water at 80 °C. After utilization, this water returns at a temperature of 60 °C and it is recirculated back to the moisture separator. The anode off gas is circulated by a blower, reheated and sent to the HER. This dried anode recycle gas leaves the anode gas recirculation and moisture separation subsystem at a fixed temperature of 460 °C in order to keep the inlet temperature of the heat exchange reformer constant throughout this study.

The efficiency of the heat transfer processes depends strongly on the choice of flow configuration and the final temperature differences between primary and secondary flows. Here, all heat exchangers are operated in counter flow mode. Only the low end temperature difference (ΔT_{low}) of the steam evaporator (apparatus 2) is set at 20 K. The others are calculated using the fixed inlet temperature of the HER

[4] See [15] for more details of fuel cell modeling.
[5] The other consumer of air is the combustion chamber of the heat exchange reformer. This amount of air is relatively small.

and the boiling temperature of water at the exchanger's outlet.

2.3. Heat exchange reformer and fuel preheat

The heat exchange reformer is modeled here by a combustion chamber and a steam-reforming reactor. The combustion chamber is fuelled by the dried anode off gas and the air factor λ of combustion is set at 1.1[6] with which flue gas at a temperature of over 1250 °C is obtained. The heat that can be derived from the flue gas is sufficient for the reforming reaction (apparatus 9, Fig. 1), superheating steam (apparatus 18) and preheating fuel (apparatus 19). The remaining heat is used for heating air (apparatus 17) that is supplied to the combustion chamber (apparatus 10). The temperature of the air leaving the heat exchanger is set at 440 °C and the temperature of both natural gas and steam that enter the HER are set at 480 °C. The natural gas heater (apparatus 19) and the steam heater (apparatus 18) are placed here in parallel since both heat exchangers are in practice combined in a single unit.

After passing the air preheater (apparatus 17), the CO_2 rich flue gas is mixed with the recycled cathode gas and preheated fresh air to provide the MCFC cathode with O_2 and CO_2.

The reforming reaction is modeled by assuming chemical equilibrium at 800 °C and 4 bar. The ratio of steam to fuel is set here to 2.59 kg/kg. Friction losses are introduced in the reformer by imposing pressure drops of 0.5 and 0.25 bar for the primary process flow (the product gas flow) and the secondary heat exchange flow (the flue gas flow) respectively. Other friction losses are introduced by pressure drops of 0.05 bar for both primary and secondary sides of the fuel preheating line. The isentropic efficiency of the air compressor is assumed to be 0.72.

2.4. Cathode gas recirculation

The cathode gas not only provides O_2 and CO_2 for the electrochemical reaction, it also serves as the main coolant for the fuel cell, and therefore the mass flow of the cathode gas has to meet the cooling requirements. This mass flow of air necessary for cooling is far greater than required for the cathode reaction. Part of this air is therefore recirculated and the amount of recirculation is set accordingly to assure the fixed cathode inlet temperature after mixing this recirculation flow with fresh air and flue gas from the HER. Before mixing, this recycle flow is partly cooled by preheating the pressurized fresh air. The flue gas from the HER is the main source of CO_2 required for the cathode reaction. In all considered situations, the concentration of CO_2 at the cathode inlet is above the commonly assumed minimum of 8 mol%.

[6] This means 10% more air than needed for stochiometric combustion.

2.5. Expander and waste heat boiler

The hot and pressurized gas that leaves the cathode recycle loop produces electricity through an expander and the attached generator. Losses are introduced by defining isentropic efficiency for the expander (here 75%) and conversion efficiency for the electrical generator (here 95%). After expansion, the temperature of the flue gas is sufficiently high to produce saturated steam. The pressure and temperature of this steam is set at 10 bar and about 180 °C. This steam can be applied for industrial heating purposes and the utilization of this heat is represented here by a heat sink. The returning condensate from this sink is used to feed the boiler. Finally, the residual flue gas is discharged to the environment via a flue gas stack.

3. Input data and calculations

The system performance depends strongly on the input data. Especially isentropic efficiencies of rotating equipment, pressure drops and pinch points of heat exchangers determine the irreversible losses of the system and therefore also the calculated overall efficiencies. For this study, we have used a combination of input data that characterize state of the art equipment. Table 2 gives the main input parameters for the components in the system.

The energy input to the system is determined by the size of the fuel cell, anode gas composition and fuel utilization. Since these parameters are fixed for all calculations, the energy input of the system is constant and in all cases the energy input is 557.57 kW, based on the lower heating value (LHV), and exergy input is 580.82 kW based on $T_0 = 25$ °C. The source for the energy and exergy input is the natural gas, which is of Dutch "Slochteren" quality with as main components about 81 mol% CH_4 and 14 mol% N_2 and with a LHV of 708.22 kJ/mol. Other mass input of this plant is air which is defined according to the ISO standard. The exact compositions that are used for both natural gas and air can be found in the handbook of the program [11].

The fuel cell system is analyzed at five different cell operating temperatures, i.e. 600, 625, 650, 675 and 700 °C. Using 650 °C as a reference, the operating temperature of the fuel cell is adjusted by changing the cell temperature and the quasi-ohmic resistance of the cell together with the change in the cathode gas recirculation percentage. Any change in the fuel cell temperature influences the quasi-ohmic resistance, which on its turn influences both cathode gas flow and the amount of the cathode gas recirculation. Consequently, the recirculation influences the cathode gas composition, which determines the quasi-ohmic resistance. All these parameters are therefore closely related and several manually controlled iterations are needed in order to find the solution for each temperature.

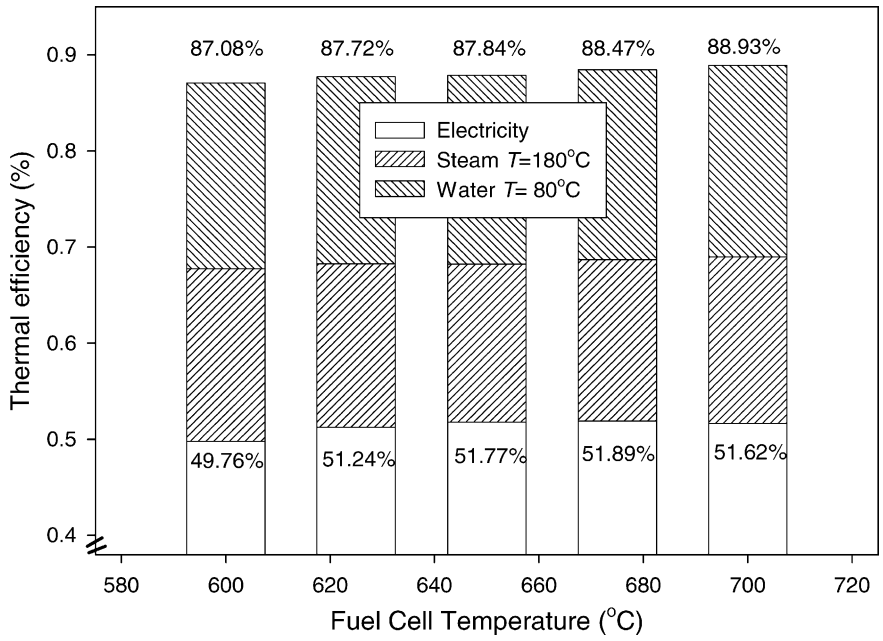

Fig. 2. Energetic efficiency and distribution as function of temperature.

4. Results and discussion

Starting with the overall results, Fig. 2 shows the overall system thermal efficiency ($\eta_{\text{total LHV}}$) and output distribution based on the energy input. Note that the surfaces in this scale do not represent the ratio of power over heat correctly since we adapted the scale to emphasize different results. The numerical values are also summarized in Table 3. Here, we should note that all numbers in the tables are given in at least two digits behind the decimal point. This suggests a high level of precision in our computer simulations. On the other hand, we have used several estimated input values for the performance of heat exchangers and rotating equipment and consequently the absolute precision in the calculated efficiencies can therefore not be guaranteed in practice. Nevertheless, these numbers are not round off in further extend since otherwise the difference in the calculated results will not become apparent. Since all calculations are based on the same system using the same system inputs, the qualitative result is therefore not affected by the estimated inputs.

Table 3
Summary of energy output

	T_{cell}				
	600 °C	625 °C	650 °C	675 °C	700 °C
P_{FC} (kW)	297.54	304.20	306.19	305.95	303.86
P_{expander} (kW)	73.86	65.60	60.05	58.64	58.20
P_{aux} (kW)	−93.98	−84.08	−77.58	−75.28	−74.22
P_{net} (kW)	277.42	285.72	288.66	289.32	287.84
$\eta_{\text{net LHV}}$ (%)	49.76	51.24	51.77	51.89	51.62
P_{steam} (kW)	100.24	94.67	91.59	93.69	96.93
P_{water} (kW)	107.86	108.68	109.49	110.28	111.06
P_{heat} (kW)	208.09	203.35	201.08	203.97	207.99
$\eta_{\text{heat LHV}}$ (%)	37.32	36.47	36.06	36.58	37.30
P_{total} (kW)	485.52	489.07	489.74	493.29	495.82
$\eta_{\text{total LHV}}$ (%)	87.08	87.72	87.84	88.47	88.93

First, we see that the electrical efficiency ($\eta_{\text{net LHV}}$) of the system increases with operating temperature and reaches a maximum at 675 °C. The difference between the maximum and minimum efficiency is about 2.1% point. Second, the overall efficiency (i.e. heat and power) increases with operating temperature as well but we did not find a peak maximum in the temperature range we investigated. In this temperature range, the difference between the maximum and minimum is here about 1.9% point. Finally, Table 3 shows that the auxiliary power consumption P_{aux} decreases with operating temperature from about 25% of the gross power production at 600 °C to about 20% at 700 °C. The auxiliary power is mainly used by the compressor for compressing fresh air for the cathode, and the change in this causes the differences in auxiliary power consumption. The rest of the auxiliary power is mainly used by the compressor for air to feed the HER and by the two recycle blowers.

Next, the causes of the changes in fuel cell power output are discussed in more detail. Fig. 3 shows the cell resistance and the net power delivered by the fuel cell stack. As expected, the irreversible losses given by the cell resistance decreases with increasing cell temperature. This results to an increase in stack performance and thus an increase in delivered power. On the other hand, the reversible open cell voltage (OCV) given by the Nernst equation decreases linearly with increasing temperature, as described in details

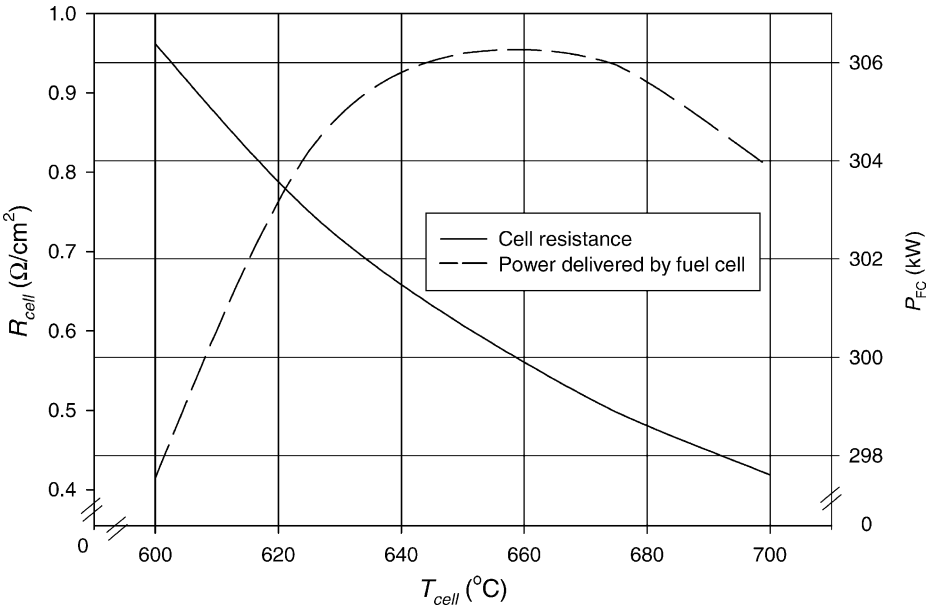

Fig. 3. Cell resistance and power delivered as function of cell temperature.

in our previous theoretical study [9]. The opposite temperature behavior of irreversible losses and OCV results here to a maximum in power output at $T_{cell} = 650\,^{\circ}C$. In our previous theoretical study [9], we did not find a maximum in cell performance in this typical range of operating temperature. There, we used a constant gas composition while in this present study the cathode gas composition is mainly determined by the cooling requirement of the stack and by the heat requirement of the cathode gas recirculation subsystem. Therefore, the exact cathode gas composition is here a function of operating temperature and this gas composition influences both the cell resistance as well as the OCV. The difference in the optimum in stack performance of our present results and our previous theoretical result can be ascribed to the differences in cathode gas composition.

The flowsheet calculations show that the overall system has a different optimum operating temperature than the fuel cell stack. This is caused by the net expander output $P_{expander}$ and auxiliary power consumption P_{aux}. We have analyzed this by examining the cell resistance and cathode recirculation data, both given in Table 4. First, we note that the difference in net performance ($\eta_{net\,LHV}$), in particular between 650 and 700 °C is very small (a difference of only 0.27%). This result is in accordance with our observation for the whole system as considered in that same theoretical study [9]. First, at low temperature, the net performance is adversely affected by the high irreversible losses while at high operating temperature the system performance remains constant. Second, high electrical output by the fuel cell should result to low heat release and consequently little cooling is required. From 600 to 650 °C, Table 4 shows a decreasing $\Phi_{cathode}$, which is a direct result of the increasing P_{FC}. It is however interesting to note that although the electrical output P_{FC} is highest at 650 °C, the cathode mass flow $\Phi_{cathode}$ and cooling requirement is lowest at 675 °C. This seems to contradict what is expected from theory, since the highest power output should result in the lowest cooling requirement. The cause of this contradiction can be ascribed to the difference in gas composition in the anode outlet due to difference in equilibrium in the hydrogen-shift reaction. At 650 °C the average enthalpy of the anode outlet is 33.31 kJ/mol (LHV) while at 675 °C it is 33.42 kJ/mol (LHV). Since the anode mass flow is constant for all calculations, the enthalpy release by anode outlet is slightly higher 675 °C. The higher enthalpy release reduces the cooling requirement of the fuel cell and hence lower cathode mass flow. The difference in

Table 4
Summary of quasi-ohmic resistance and cathode recirculation

	T_{cell}				
	600 °C	625 °C	650 °C	675 °C	700 °C
r (Ω cm^2)	0.9619	0.7501	0.6072	0.4976	0.4187
$\%_{recirculation}$	72.83	75.02	77.09	78.00	78.84
$\Phi_{cathode}$ (kg/s)	1.383	1.304	1.267	1.256	1.262
$\Phi_{expander}$(kg/s)	0.344	0.297	0.264	0.251	0.243

Table 5
Summary of exergy output (with $T_0 = 25\,^{\circ}C$)

	T_{cell}				
	600 °C	625 °C	650 °C	675 °C	700 °C
Ex_{net} (kW)	277.42	285.72	288.66	289.32	287.84
Ex_{steam} (kW)	36.48	34.46	33.34	34.10	35.28
Ex_{water} (kW)	17.27	17.41	17.54	17.66	17.79
η_{Ex} (%)	57.02	58.12	58.46	58.72	58.69

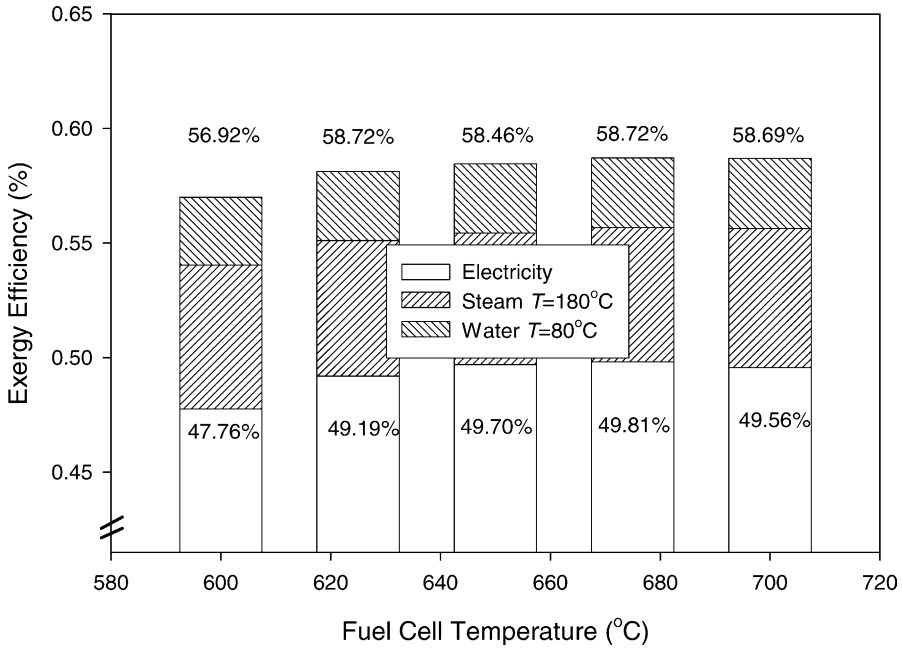

Fig. 4. Exergetic efficiency and distribution as function of temperature.

cathode mass flow turns the optimum temperature for the system to 675 °C from the optimum temperature of 650 °C for the stack. Finally, this study also shows that operating at elevated temperature requires increase in cathode recycling due to the higher inlet temperature of the fuel cell. This is shown in Table 4 where the recirculation percentage of the cathode gas $\%_{\text{recirculation}}$, cathode mass flow Φ_{cathode} and expander mass flow Φ_{expander} are given. The increase in $\%_{\text{recirculation}}$ reduces expander power output and the overall auxiliary power consumption. The latter is due to the lower air input and less work required for the compression of air.

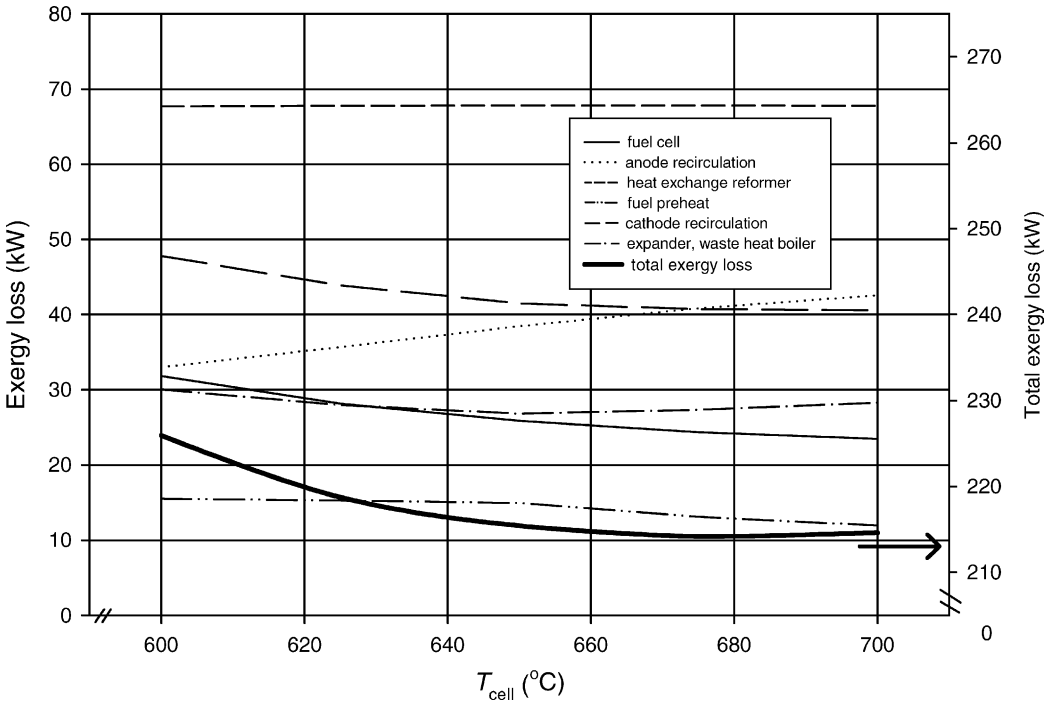

Fig. 5. Exergy loss of subsystems as function of temperature.

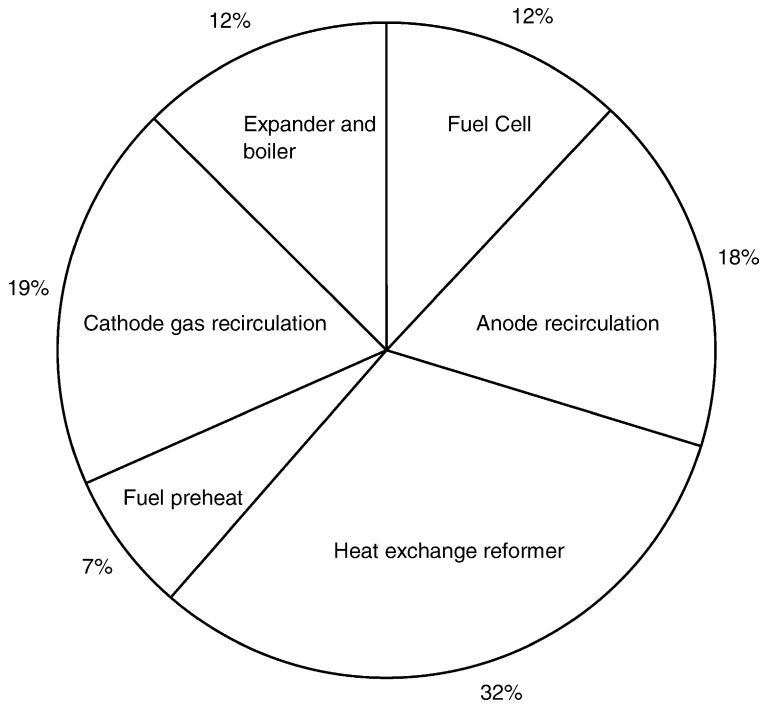

Fig. 6. Exergy loss distribution at the typical operating temperature of 650 °C.

Table 3 gives the overall results and it lists the amount of useful heat produced by the system that is consumed by external users. The production of hot water at 80 °C increases monotone with operating temperature while the steam production at 180 °C shows a minimum at 650 °C. The change of the latter dominates the overall heat production resulting in a minimum total heat production (P_{heat}) of 201.08 kW at 650 °C. The overall efficiency η_{total} (i.e. combined electricity and heat) increases monotone with operating temperature. We should note that the main purpose of the fuel cell plant is the production of electricity while the production of heat is of minor importance. This is more apparent when we evaluate this system based on exergy. Fig. 4 shows the exergetic efficiency and exergy output distribution of the system (note the scale of this figure). The numerical values are summarized in Table 5. It is clear that the exergy represented by the produced heat is relatively small. Based on exergy, the system efficiency η_{EX} shows a maximum at 675 °C. The difference in overall exergetic efficiency between the highest and lowest value is here 1.7%. Again, the change in exergy efficiency in the temperature range between 650 and 700 °C is small.

Furthermore, we have analyzed the exergy loss of the subsystems and their temperature dependency and this is shown by Fig. 5. It shows that the exergy loss of the subsystems HER, fuel preheat and expander, waste heat boiler are little temperature dependant. The exergy loss of the fuel cell and cathode recycling decreases while the anode recycling increases with operating temperature. The overall result is a minimum of exergy loss at 675 °C and thus an optimum in overall exergy efficiency.

Finally, Fig. 6 shows the exergy loss distribution at the typical operating temperature of $T_{cell} = 650$ °C. It shows that the HER has the highest contribution to the total exergy loss. The combustion process of the HER is the main cause of the exergy loss of this system (about 65%) while the contribution from heat transfer to the reforming reaction is relatively small (the remaining 35%). Improvement in system efficiency is therefore expected when changing this external reforming configuration to internal reforming. This off course will involve different MCFC stack technology and eventually will affect the system layout.

5. Conclusion

The influence of the operating temperature of the fuel cell on the overall system efficiency is small in the operating range between 650 and 700 °C. This result is in accordance with the results of our previous study [9]. This fuel cell system performs best at 675 °C with a net electrical efficiency of 51.89% point (based on LHV). This is the main conclusion since the production of electricity is the objective while the production of heat is of minor importance. Production of heat plays a role when this system is integrated to industrial processes together with district heating system. Exergy conservation is then an additional requirement for a sustainable society. The exergetic efficiency of this system is at maximum as well at 675 °C with a value of 58.72%. The overall energetic CHP efficiency based on LHV increases with operating temperature and the highest value is achieved at the highest temperature considered.

The exergy loss contributed by the heat exchange reformer is the highest of all subsystems and this should be tackled case of further system optimization.

The conclusions regarding the efficiencies as function of operating temperature as presented here are restricted to this specific plant design. Nevertheless, the present study has shown the complexity of a fuel cell system. The refinement by detail flowsheet analysis as presented here has revealed interactions between subsystems that cannot be seen otherwise. Examples are the different optimum temperature for the fuel cell and overall system and the mismatch between the optimum stack temperature and the minimum stack-cooling requirement. Furthermore, we have shown the complex interactions between the different processes in a system. We have seen here that changes in cell temperature involve the following changes: (1) reversible heat production and irreversible losses of the fuel cell; (2) cooling requirement of the cell and consequently the auxiliary power consumption; and (3) changes in recirculation mass flows due to the changes in fuel cell inlet temperature. Their relation can only be made visible by flowsheet calculations. This study has therefore shown the importance of flowsheet calculation during the evaluation of the complete fuel cell plant when changing process parameters. Simple theoretical calculations can show first order trends but detailed flowsheet calculations are required due to the complex behavior and intricate interactions in a fuel cell plant.

References

[1] J.H. Hirschenhofer, D.B. Stauffer, R.R. Engleman, Fuel Cells—A Handbook, Revision 3, Gilbert/Commonwealth for the US Department of Energy, Contract No. DE-AC01-88FE61684, 1994.

[2] K. Ota, K. Toda, S. Mitsushima, N. Kamiya, Accerated corrosion of stainless steels with presence of molten carbonate below 923 K, Bull. Electrochem. Soc. Jpn. (2002) 877–881.

[3] C.G. Lee, Y. Kohta, T. Nishina, I. Uchida, In situ NiO dissolution behavior in (Li + Na)CO_3 melts under pressurized oxidant gas atmospheres, J. Power Sources 62 (1996) 145–147.

[4] F.R.A.M. Standaert, Analytical Fuel Cell Modeling and Exergy Analysis of Fuel Cells, Ph.D. Thesis, Delft University of Technology, The Netherlands, 1998.

[5] E. Arato, B. Bosio, R. Massa, F. Parodi, Optimisation of cell shape for industrial MCFC stacks, J. Power Sources 86 (2000) 302–308.

[6] F. Yoshiba, N. Ono, Y. Izaki, T. Watanabe, T. Abe, Numerical analyses of the internal condition of a molten carbonate fuel cell stack: comparison of stack performances for various gas flow types, J. Power Sources 71 (1998) 328–336.

[7] F. Standaert, K. Hemmes, N. Woudstra, Nernst loss, mutistage oxidation in fuel cells, in: Proceedings of the Fuel Cell Seminar, 16–19 November 1998, Palm Spring, CA, USA, 1998, pp. 92–95.

[8] B.S. Kang, J.H. Koh, H.C. Lim, Effect of system configuration and operating condition on MCFC system efficiency, J. Power Sources 108 (2002) 232–238.

[9] S.F. Au, K. Hemmes, N. Woudstra, The influence of operating temperature on the efficiency of combined fuel cell and power cycle system, J. Electrochem. Soc. 149 (7) (2002) A879–A885.

[10] S.F. Au, K. Hemmes, N. Woudstra, in: Proceedings of the Abstracts of the 200th Meeting of the Electrochemical Society, Number 0455, 2001.

[11] Cycle-Tempo version 4.42, Section of Thermal Power Engineering TNO Environment, Energy and Process Innovation, Delft University of Technology, The Netherlands, 2000, http://www-pe.wbmt.tudelft.nl/ev/cycle/cycle.html.

[12] P.C. van der Laag, T.W. Verbrugge, in: Proceedings of the 1994 Fuel Cell Seminar-Program and Abstracts, 1994, pp. 152–155.

[13] S.F. Au, W.H.A. Peelen, F.R.A.M. Standaert, K. Hemmes, I. Uchida, Verification of analytical fuel cell models by performance testing at a 110 cm^2 molten carbonate fuel cell, J. Electrochem. Soc. 148 (10) (2001) A1051–A1057.

[14] S.F. Au, N. Woudstra, K. Hemmes, I. Uchida, Verification of a simple numerical model in a flowsheeting program by performance testing at a 110 cm^2 molten carbonate fuel cell, Energy, Conversion Management, in press.

[15] Y. Mugikura, H. Morita, M. Yoshikawa, T. Watanabe, Modification of cathode performance equation and reaction mechanism of MCFC, in: Proceeding of the Seventh FCDIC Fuel Cell Symposium, Tokyo, Japan, 2000.